Terrain Roughness Identification for High-Speed UGVs

Graeme N. Wilson, Alejandro Ramirez-Serrano
University of Calgary
2500 University Dr NW, Calgary, T2N 1N4, Canada
gnw.wilson@gmail.com; aramirez@ucalgary.ca

Abstract - High-speed navigation of autonomous Unmanned Ground Vehicles (UGVs) in rough unknown terrains requires the detection and identification of the terrain in order to make effective navigation decisions. This paper investigates a geometrical approach to identifying terrain based on its roughness using the terrain elevations from a point cloud generated using a 3D camera. This roughness, called the Roughness Index (RI), is used to identify different terrains by overlaying the terrain with a grid map and using the standard deviation of the point cloud elevations in each grid cell. The experimental testing and results of this terrain identification technique are presented as determined from field experiments using an experimental UGV test platform on rough outdoor terrains.

Keywords: Terrain classification, unmanned ground vehicles, terrain identification, terrain roughness detection.

1. Introduction

Unmanned Ground Vehicles (UGVs) are becoming increasingly prevalent in everyday life as these complex systems are being used in applications including surveillance, military, law enforcement, industrial hauling, and search and rescue. In order for these systems to navigate effectively in any environment they must be able to detect the terrain and react accordingly.

This paper investigates the challenge of terrain identification for use in making navigation decisions. Previous work in this area has investigated binary classification to solve this problem where terrain is classified into traversable and non-traversable regions (Kim D., et al., 2007).

The problem with binary approaches is that the degree of traversability is not determined (e.g. pavement and gravel are both traversable, but pavement is more traversable). Reactive multi-class terrain classification attempts to solve this problem by classifying terrain into multiple categories (e.g. grass, gravel) based on the vibrational acceleration imparted by the terrain using trained machine learning techniques such as Neural Networks (Collins E. G. and Coyle E. J., 2008), Principle Component Analysis (DuPont E. M., et.al, 2006), and Support Vector Machines (Weiss C., et al., 2007).With reactive techniques the terrain must be encountered before the classification is made, and if the UGV is traveling at high-speed this could cause damage. To identify terrain before encountering it predictive multi-class terrain classification has been investigated. These approaches use machine learning to train visual classifiers to identify terrain based on appearance using standard cameras (J. Kim, et al., 2009), laser scanners (Lu L., et al., 2011), and stereo cameras (Talukder A., et al., 2002). These predictive techniques have been improved even further by incorporating the reactive vibrational classifications to train the visual classifiers both offline (Komma P., et al., 2009), and online (Brooks C. A. and Iagnemma K., 2012).

The problem with these machine learning classifiers is that they may perform poorly if a new type of terrain is encountered, and that training can take substantial time. Geometric based terrain classification approaches attempt to solve this by classifying terrain based on its geometric appearance from a point cloud generated by 3D cameras (e.g. stereo cameras, 3D laser scanners) (Howard A. and Tunstel E., 2006). A promising approach proposed by El-Kabbany and Ramirez-Serrano (2010) identified terrain using terrain roughness detection; improvements on their approach are proposed by Wilson et al. (2012). This paper further explores the approach developed by Wilson et al. (2012) through detailed real-world

experimental testing and implementation of the terrain roughness detection technique called the Roughness Index (RI). This is done on rough outdoor terrain using an experimental UGV platform.

2. Theory

Traversing a given *a priori* unknown terrain effectively with a UGV requires the perception of the terrain in front of the UGV. In this article this is accomplished through geometric perception of the terrain using a range sensor (e.g. stereo camera, 3D laser scanner) to produce a point cloud; experimental tests in this article used a MESA SwissRanger SR4000 3D camera. As a 3D point cloud itself is not directly useful for navigation decision making, this data must be processed to identify the terrain based on its geometrical properties. For this purpose the Roughness Index (RI) was developed. The RI is used to identify the perceived roughness of a terrain using a 3D point cloud; the RI is defined as follows:

$$RI = \frac{s_e}{h} = \frac{1}{h}\sqrt{\sum_{i=1}^{n}\frac{(e_i - \bar{e})^2}{n-1}} \tag{1}$$

where s_e is the sample standard deviation of the point elevations for a sample of size n, e_i is a point elevation in the sample, $\bar{e}$ is the sample mean of the point elevations, and h is the ground clearance of the UGV.

The reason for the inclusion of the ground clearance h in Equation (1) is for the comparison of roughness relative to the capabilities of the UGV. While mathematically the RI has a range of $[0, \infty)$, where 0 is a perfectly smooth terrain and ∞ is the roughest possible terrain, in practice it can be generally visualized that any terrain with $RI \approx 0$ is smooth, while any terrain with $RI \approx 1$ is rough. The selection of 1 as rough terrain is arbitrary, though mathematically it means that ~32% of the terrain point elevations are at least one ground clearance greater than the mean (which is a significant elevation change).

To demonstrate how the RI works a simulated example of a UGV identifying a sigmoid terrain is presented. In this example the ground clearance h of the vehicle was set to $0.1\ m$, while the terrain elevation change was $0.15\ m$. The surface of the sigmoid terrain being identified is shown in Figure 1, while the sigmoid terrain profile is compared to the vehicle in Figure 2.
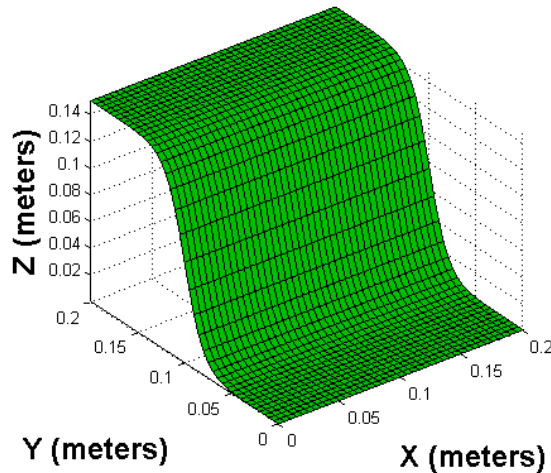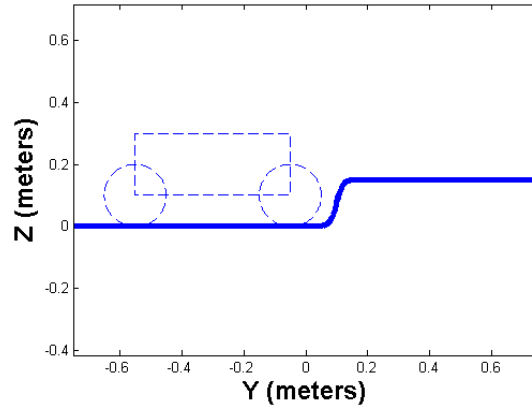

Fig.1. Sigmoid surface.

Fig. 2. Sigmoid Compared to UGV.

To obtain a point cloud that represented this terrain 200 random points were placed on the surface of the sigmoid (Figure 3 & Figure 4) and from these the RI was calculated. For these points the mean terrain point elevation was $0.79\ m$ and the RI was 0.66. From these numbers it can be seen that a terrain with an $RI \approx 1$ would be quite rough supporting the proposal that a value of 1 can be considered rough terrain for visualization purposes.

3. Implementation

When implementing the RI for the purpose of terrain identification on a UGV one possibility is to use the entire point cloud to calculate a single RI for the entire area being captured by the 3D camera. The problem with this is that different areas of the terrain that are being captured may have dramatically different roughness. In the case of the MESA SwissRanger SR4000 the range of the camera is ~10m; this is a long distance where roughness may not be uniform. To improve the terrain identification the terrain can be divided into a 2D grid map where the dimensions are the horizontal distance in front of the camera, and the horizontal distances to the left and right of the camera. For each grid cell the RI can be calculate individually using the mean of the terrain elevation points within each cell.
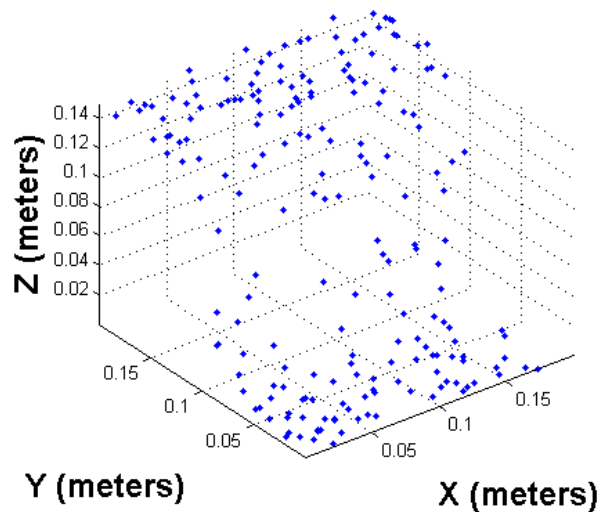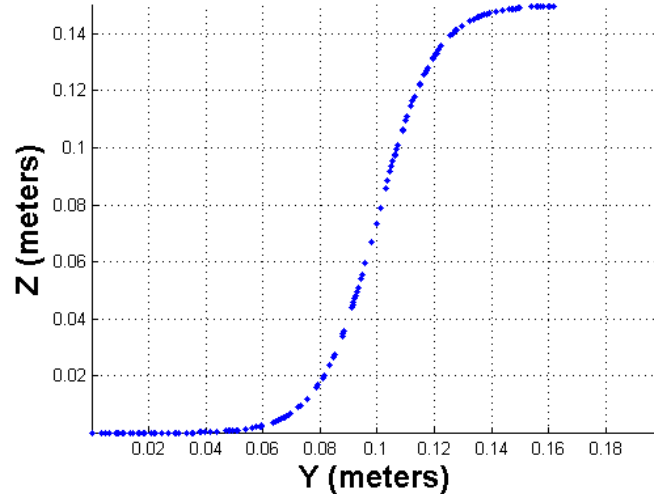

Fig. 3. Point cloud.

Fig. 4. Point cloud: side view.

For this 2D grid approach to implementing the RI it is important to take into account the number of terrain elevations points that are sampled in each grid cell. Since the RI is calculated as the sample standard deviation of the terrain point elevations it is important that this sample standard deviation be representative of the population standard deviation of the grid cell. For this purpose assume that the terrain point elevation population follows a normal distribution in each grid cell. Since each grid cell contains a sample of the terrain point elevation population consider the t-distribution that describes the distribution shape as a function of the sample size. As the sample size approaches ∞ the t-distribution is equal to the normal distribution, and therefore at a sufficiently large sample size the t-distribution is a good approximation of the normal distribution. A common arbitrarily selected value for this approximation is a sample size of 30 (McClave J. T. and Sincich T., 2009). Therefore in this article it is assumed that if the sample size of the terrain elevation points in a grid cell is ≥ 30 then the sample standard deviation is considered to be a sufficient approximation of the population standard deviation. In the implementation of the RI in a 2D grid map any cell with less than 30 points is labeled as invalid.

Given that it is assumed that ≥ 30 terrain elevation points are needed in a grid cell for it to be valid, it is important to consider the size of the grid cells. If the grid cells are made too small most of the grid cells will have < 30 terrain elevation points and will be invalid. On the other hand, if the grid size is too large then smaller details about the terrain will be lost. It is therefore important to select an appropriate grid cell size based on the cameras resolution. To observe the effect of grid size on the RI grid, consider the terrain presented in Figure 5. Using a SR4000 3D camera a point cloud of the terrain was obtained (Figure 6).
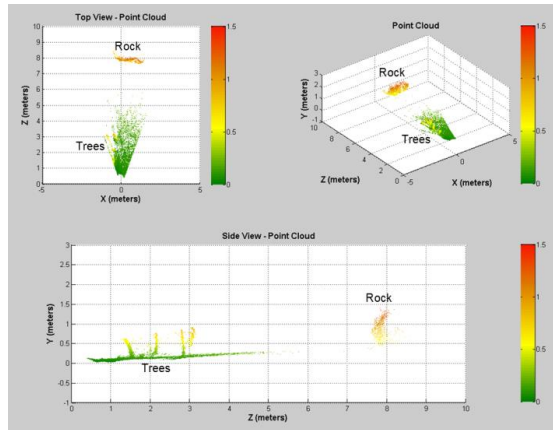

Fig. 5. Complex terrain.

Fig. 6. Complex terrain point cloud.

From the point cloud in Figure 6 RI grids for various grid sizes were calculated. These grid sizes were $0.05m$, $0.1m$, $0.2m$, $0.5m$, and $1.0m$ as shown respectively in Figure 7 through Figure 11.
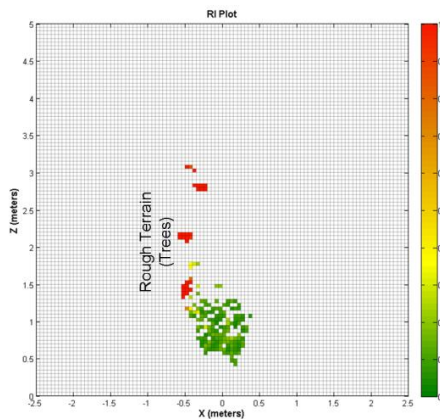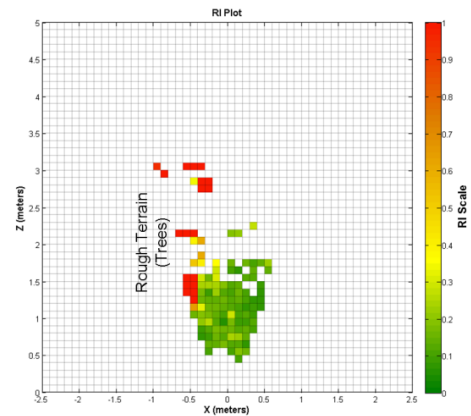

Fig. 7. Grid size 0.05m.
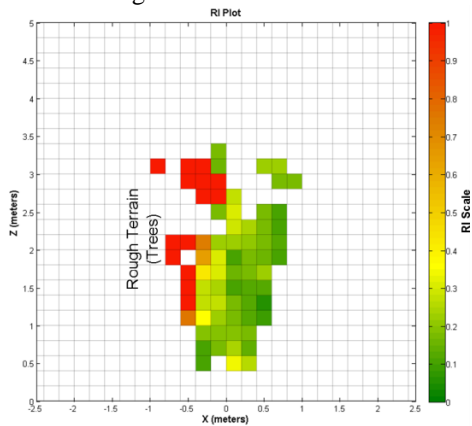

Fig. 8. Grid size 0.1m.
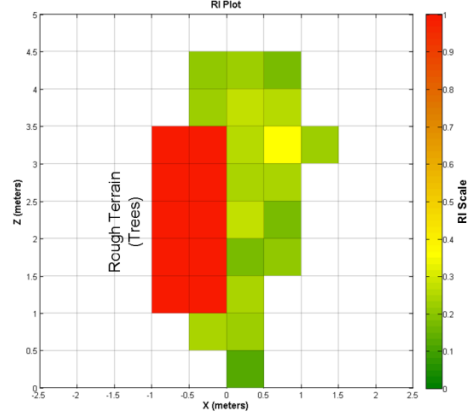

Fig. 9. Grid size 0.2m.
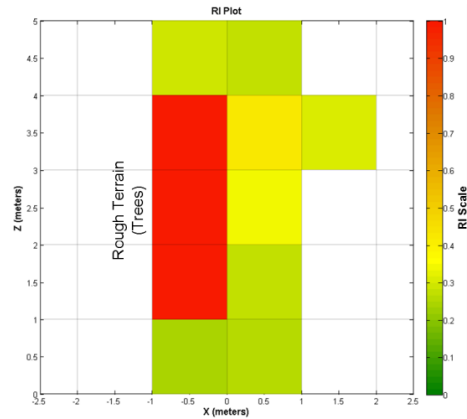

Fig. 10. Grid size 0.5m.

11-5

Fig. 11. Grid size 1.0m.

Observing Figure 7, that has the lowest grid size, it is clear that due to the point density of the camera there are limited areas of the image which have ≥ 30 points; therefore, other than a couple high roughness obstacles (trees) only about 1 to $1.5m$ of the terrain has any RI associated with it. In Figure 8, with a $0.1m$ grid size, the range at which there is RI information has been extended to about 1.5 to $2.0m$, and the individual obstacles (trees) are still clearly visible. When the grid size reaches $0.2m$ in Figure 9 the trees have begun to be lumped together into larger areas of high RI, though at the same time the patches of trees are still separated into two areas. This grid size has extended the range of RI identified areas to about 2.5 to $3.0m$. When the grid size is increased yet further to $0.5m$ as shown in Figure 10 the trees have become a single area of high roughness and all fine details have been lost. The advantage to this grid size is that the range of the RI grid has been increased to about $4.5m$. With the largest grid (Figure 11) it can be seen that the RI scores have become generalized and there are no areas which have less than a 0.2 RI score. With this large grid size there are no fine details remaining about the terrain; however, the range of areas with RI scores is the largest (extending the full $5m$).

From Figure 7 to Figure 11 it can be seen that it is important to have a compromise between RI grid range and the resolution of the RI grid. If the grid size is too small there will be very few areas with an RI since < 30 points fall in the majority of the grid cells. If the grid cell size is too large fine details about the terrain are lost, and the areas that do exist become more generalized as they are taking the standard deviation of points over a larger area. For the purpose of the testing in this article a grid cell size of $0.2m$ was selected for use.

4. Experimental Platform

For the experimental testing of the RI in outdoor terrains on a moving UGV an experimental test platform had to be developed. This custom test platform is shown in Figure 12.
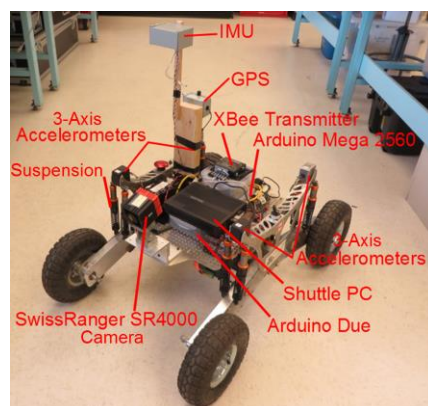

Fig. 12. Experimental test platform.

This vehicle was custom made for the AR^{2}S Laboratory running a multitude of sensors for terrain identification and vehicle state estimation. The state of the vehicle (position, velocity, orientation) is estimated using an IMU, GPS, and wheel encoders running various algorithms including a Kalman filter for positioning data. The SwissRanger SR4000 mounted on the front of the vehicle is the 3D camera which captures the point cloud. The Arduinos handle the motor control and the sensor data acquisition while the Shuttle PC collects, processes, and stores the experimental data. The UGV was driven by remote control where the XBee wireless transmitter received the motion commands. This vehicle had a ground clearance of $0.09m$.

5. Experimental Testing and Results

During the experimental testing the UGV was driven at a speed of ~1.5m/s. During the testing the point cloud of the terrain was captured and stored in real time along with the vehicle state estimates in 10 to $20m$ tests. For the testing the UGV was driven through a variety of terrains including roots, pavement, gravel, and grass (Figure 13 to Figure 16).

After the data was gathered it was processed in the lab to produce the RI in a graphical RI grid map. The processing time of the point clouds for each run into RI grids took approximately $1/5$ of the time each experiment was run (i.e. 25s test run takes 5s to process and plot). This means this terrain identification technique is suitable for real-world applications since it is able to run in real-time. The results for each of the terrains are shown below (Figure 17 to Figure 20).

Fig. 13. Root terrain.

Fig. 14. Pavement terrain.

Fig. 15. Gravel terrain.

Fig. 16. Grass terrain.

From Figure 17 through Figure 20 it can be seen that the Root terrain (Figure 17) is the roughest RI grid (as expected), while the other three terrains are more similar in appearance. It can be noted that the pavement (Figure 18) and gravel (Figure 19) terrains are almost identical in appearance, which is to be expected since they are both relatively smooth and hard surfaces. It should be mentioned that especially in the gravel terrain there are some isolated areas of high roughness. These areas are attributed to artifacts introduced by the parking lot lighting. It was noticed that streetlights caused errors in the SwissRanger SR4000 cameras point cloud; presumably the wavelength of the light being output by the lights is the

same as that of the SR4000's TOF sensors. The grass terrain (Figure 20) was slightly different than the pavement and gravel, having areas of moderate roughness (RI≈0.5). This is because the grass, instead of the ground underneath, is being detected by the SR4000 and the point cloud is producing a rougher appearing terrain than actually exists. This is an issue with all current sensors and deformable terrain/vegetation. Current sensor technology and techniques have a very difficult time dealing with obstructions and terrain such as tall grass.

Addressing the most dynamic terrain again, the root terrain (Figure 21), observe a comparison of different areas of the terrain in Figure 22. The first area labelled Area 1 corresponds to a large horizontal root. As expected, in the RI grid this is detected as a feature. Area 2 is a large wide collection of roots that is also detected properly in the RI grids as a large area of high roughness. Finally, Area 3 is a smoother area of dirt that is also correctly identified in the RI grid. From this it is concluded that the RI is performing properly and correctly identifying areas of high and low roughness.
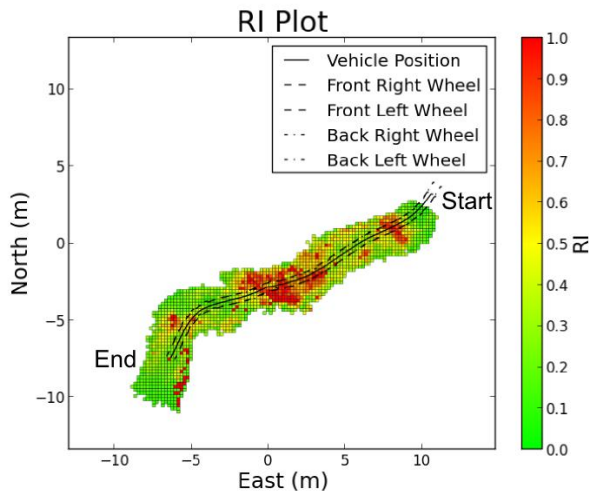
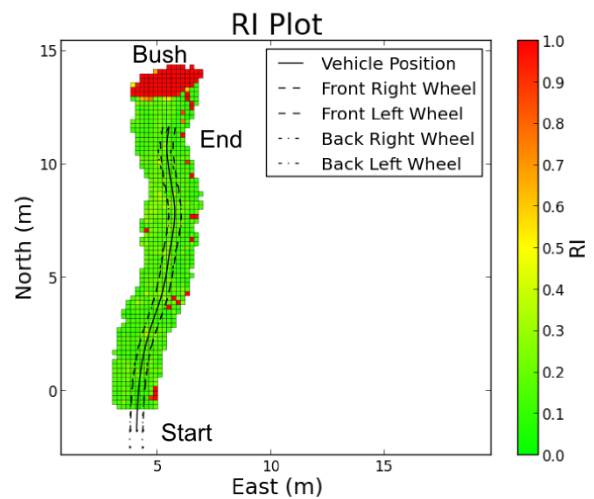
Fig. 17. Root RI grid.

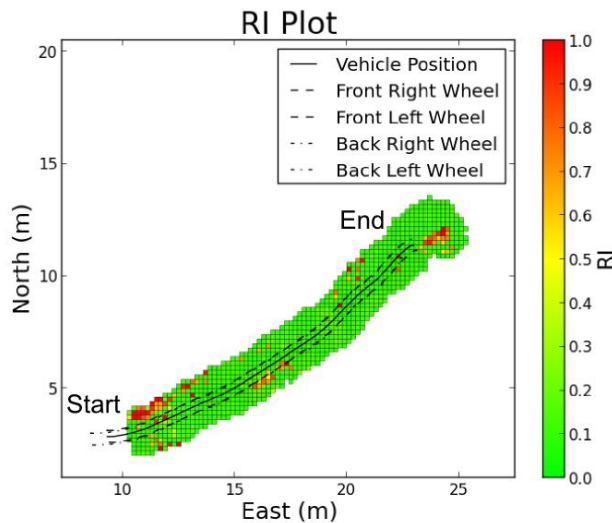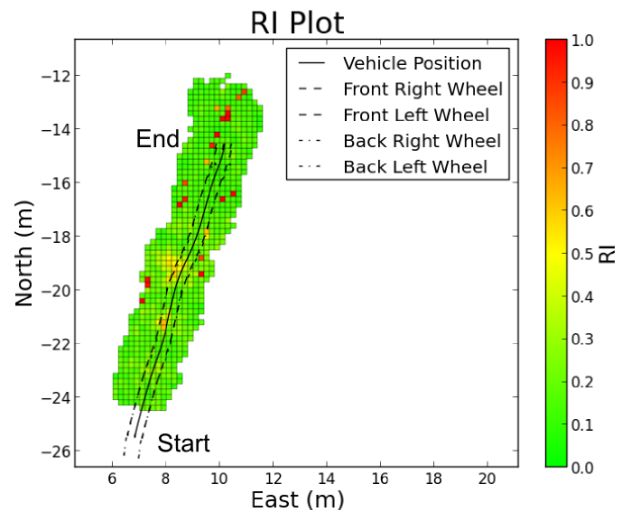Fig. 18. Pavement RI grid.

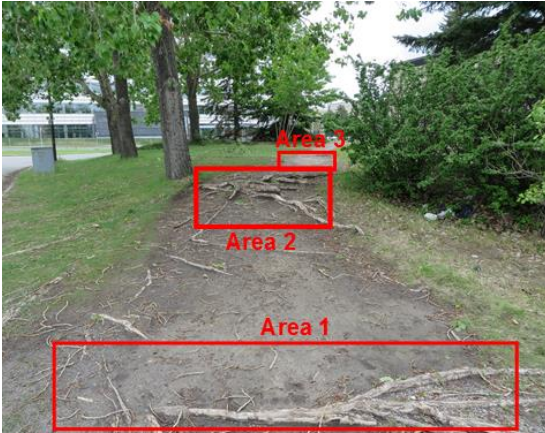Fig. 19. Gravel RI grid.

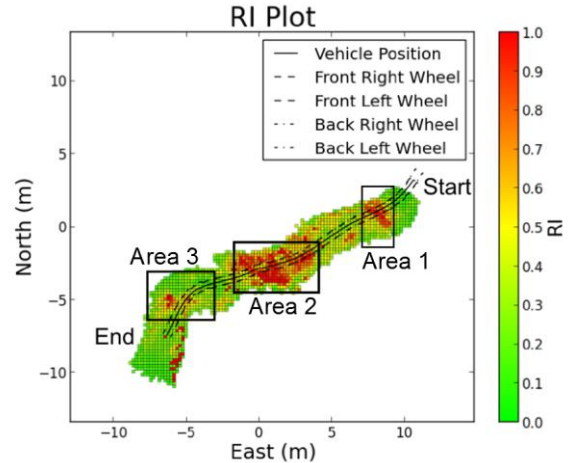Fig. 20. Grass RI grid.

Fig. 21. Labeled root terrain.

Fig. 22. Labeled RI grid.

6. Conclusion

This paper presented a geometrical terrain identification approach, the Roughness Index (RI), that identified terrain based on the roughness of the terrain using the point cloud of a 3D camera sensor. Techniques for implementing the RI on real world terrains using a grid map were investigated. Comparisons of different grid size selections and their effect on the RI grid map were discussed. It was found that as the grid size was increased the effective range of the 3D camera was increased (due to the sparsity of points at longer ranges); however, this range increase came at the cost of losing terrain details. It was therefore concluded that a compromise must be selected between RI grid range and the detailed resolution of the grid.

This technique was also implemented on an experimental UGV platform for real-world testing. During the testing the RI was computed for a variety of terrains (grass, gravel, pavement, roots). It was found that the RI performed well at correctly identifying areas of high and low roughness. It was also concluded that the algorithm was fast enough to run in real time for high-speed vehicles, meaning it can be used in real-world applications.

Further work in this area includes expanding this roughness detection to account for terrain deformability (the technique proposed here assumes all terrain is rigid), and extrapolating terrain roughness to distant terrain using terrain appearance in a camera image (since 3D point cloud generating sensors are either short range or have low point density at long ranges).

References

Brooks C. A. and Iagnemma K. (2012). Self-Supervised Terrain Classification for Planetary Surface Exploration Rovers. "J. of Field Robot" vol. 29, no. 3, pp. 445–468.

Collins E. G. and Coyle E. J. (2008). Vibration-Based Terrain Classification Using Surface Profile Input Frequency Responses. "IEEE Int. Conf. on Robot. and Autom" pp. 3276–3283.

DuPont E. M., Roberts R. G., and Moore C. A. Speed Independent Terrain Classification. (2006). "Proc. of the 38th Southeastern Symp. on System Theory" pp. 240–244.

El-Kabbany A. and Ramirez-Serrano A. (2010). Terrain Roughness Assessment for High Speed UGV Navigation in Unknown Heterogeneous Terrains. "Int. J. of Inf. Acq." vol. 7-2, pp. 165–176.

Howard A. and Tunstel E. (2006). A Self-Contained Traversability Sensor for Safe Mobile Robot Guidance in Unknown Terrain. "Advances in Intell. and Soft Computing" vol. 34, pp. 731–748.

Kim D., et al. (2007). Traversability classification for UGV navigation: a comparison of patch and superpixel representations. "IEEE/RSJ Int.Conf. on Intel. Robots and Systems" pp. 3166–3173.

Kim J., et al. (2009). Non-contact Terrain Classification for Autonomous Mobile Robot. "Proc. of the 2009 IEEE Int. Conf. on Robotics and Biomimetics" pp. 824–829.

Komma P., Weiss C., and Zell A. (2009). Adaptive Bayesian Filtering for Vibration-based Terrain Classification. "IEEE Int. Conf. on Robotics and Automation" pp. 3307–3313.

Lu L., et al. (2011). Terrain surface classification with a control mode update rule using a 2D laser stripe-based structured light sensor. "Robotics and Auton. Systems" vol. 59, no. 11, pp. 954–965.

McClave J. T. and Sincich T. (2009). "Statistics 11th ed.". Pearson.

Talukder A., et al. (2002). Autonomous Terrain Characterisation and Modelling for Dynamic Control of Unmanned Vehicles. "Proc. of the IEEE/RSJ Int. Conf. on Intel. Robots and Sys." pp. 708–713.

Weiss C., Stark M., and Zell A. (2007). SVMs for Vibration-Based Terrain Classification. "Autonome Mobile Systeme" pp. 1–7.

Wilson G. N., et al. (2012). Velocity Selection for High-Speed UGVs in Rough Unknown Terrains Using Force Prediction. "Proc. of 5th Int. Conf. on Intel. Robot. and App." pp. 387–396.